

Synthesis of Chromium Doped Cobalt Oxide (Cr:Co₃O₄) Nanoparticles by Co-Precipitation Method and Enhanced Photocatalytic Properties in the Visible Region

Hitkari G, Sandhya S, Gajanan P, Manoj K Shrivash and Deepak Kumar*

Department of Applied Chemistry, Babasaheb Bhimrao Ambedkar University, Lucknow, India

Abstract

In the present work, Co₃O₄, 1% chromium doped Co₃O₄ (1% Cr:Co₃O₄), and 5% chromium doped Co₃O₄ (5% Cr:Co₃O₄) was successfully prepared by simple chemical co-precipitation method followed by calcination at 400°C for 3 h. The synthesized nanoparticles materials were characterized by X-ray diffraction (XRD), scanning electron microscope (SEM), energy dispersive X-ray spectroscopy (EDX), Brunauer Emmett Teller analysis (BET), and UV-visible spectroscopy. XRD confirmed the formation of cubic nature of nanoparticles while SEM images shown spherical structure. BET analysis confirmed the mesoporous behaviour of nanoparticles. UV-Visible spectra have been used to determine band gap and photo-oxidation behaviour of organic dye methyl orange. Experimental data suggested that 5% Cr:Co₃O₄ nanoparticles catalyst possessed the highest catalytic activity towards MB degradation in aqueous solution at the tested concentration level of 50 mg/L, higher than that of pure Co₃O₄.

Keywords: Nanoparticle; XRD; SEM, EDX; BET

Introduction

From the several last decades, more attentions have been paid for the preparation of nanocrystalline materials with appropriate size, geometry and stoichiometry to enhanced the magnetic activity as compare to their bulk counterpart. Essentially, chemical composition, distribution of cation, shape and size of the particle are responsible for change in morphology and various properties [1-4]. There are new opening corridor of advanced properties of the particles like detection of hazardous gasses, spintronic equipment, magnetic seals, biomedical application [5] and photo-disappearance of organic toxic pollutants by photocatalysis as well as easily magnetic recoverable photocatalyst [6-9]. As reduction in the size of particle into nanometre scale, then its surface consequence develops into more and more important due to the enhancing fraction of surface atoms, and the symmetry of the crystal is diminished for those metallic cations which accommodated on the surface because of the occurrence of incomplete atomic coordination.

Among the magnetic materials, oxides of transition metal with spinel structure are one of the most important magnetic materials [10], the generalised formulation for the magnetic spinel can be denoted as AB₂O₄ (A=Zn, Fe, Co, Ni, Mg, etc.; B=Fe, Cr, Mn, Al, etc.), where A and B symbolizes the divalent and trivalent cat ions, respectively. The coordination of the presented ions at both A and B sites can be tetrahedral and octahedral with oxygen atoms. The magnetic performance of these compounds is very conscious of the nature of cations and their distribution among the two interstitial sites of spinel lattice, that it can be adjusted through modulation of cat ion composition and cat ion distribution [11]. Cobalt oxide (Co₃O₄) is a normal spinel among the transition metal oxide with crystal structure established on a cubic close packing array of oxide ions, in which Co (II) ions occupy 1/8 tetrahedral A sites and Co (III) ions occupy 1/2 octahedral B sites. Moreover, Co₃O₄ is an intrinsic p-type semiconductor with extraordinary awareness because of its prospective applications as heterogeneous catalysts, sensors, electrochemical devices, lithium ion batteries and magnetic materials. Lou et al. described the photo catalytic behaviour of Co₃O₄ nano rods synthesized by the complex pyrogenation technique for the elimination of organic contaminants in water. Co₃O₄ is also a capable applicant for the utilization in high-

power lithium ion batteries, because of its outstanding rate ability and good cycle life [12].

There is numerous type of methods have been described for the preparation of Co₃O₄ nanoparticles, He et al. used solubility controlled method for the production of Co₃O₄ nano crystals by applying surfactant [13], Gu et al. have also been reported facile combustion method for the preparation of Co₃O₄ nanocrystals [14]. A lot of different methods have also been applying for the fabrication of spinel Co₃O₄ nano crystals like as polyol process, a sol-gel method, polymer assisted synthesis, solvothermal synthesis, thermal decompositions and hydrothermal synthesis for Co₃O₄ nanorods [15-20].

In the present paper, we have employed a simple co-precipitation method to achieve nano-sized chromium doped cobalt oxide (Cr:Co₃O₄) nanoparticles and their photocatalytic activity was checked out by applying methylene blue (MB) dyes as toxic materials under the radiation of visible light. This method does not require any type of special conditions such as a special surfactant, or temperature and pressure controlling. The character of the as-synthesized material was characterized by X-ray diffraction (XRD), Scanning Electron Microscopy (SEM), Ultraviolet-visible spectroscopy and BET techniques.

Experimental Section

Chemicals and materials

Analytical grade cobalt chloride hexahydrate (CoCl₂·6H₂O, Merck

*Corresponding author: Deepak Kumar, Research Scholar, Department of Applied Chemistry, Babasaheb Bhimrao Ambedkar University, Lucknow, India, Tel: 9412818506; E-mail: dpk.4470@yahoo.in

Received December 13, 2017; Accepted January 23, 2018; Published February 05, 2018

Citation: Hitkari G, Sandhya S, Gajanan P, Shrivash MK, Deepak K (2018) Synthesis of Chromium Doped Cobalt Oxide (Cr:Co₃O₄) Nanoparticles by Co-Precipitation Method and Enhanced Photocatalytic Properties in the Visible Region. J Material Sci Eng 7: 419. doi: [10.4172/2169-0022.1000419](https://doi.org/10.4172/2169-0022.1000419)

Copyright: © 2018 Hitkari G, et al. This is an open-access article distributed under the terms of the Creative Commons Attribution License, which permits unrestricted use, distribution, and reproduction in any medium, provided the original author and source are credited.

India), chromium chloride hexahydrate (CrCl₂·6H₂O, Himedia India), methylene blue (MB) and ammonia solution (Merck India) were used without any further purification. Doubled de-ionized water was used as a solvent. All the glassware's were cleaned with concentrated acid. The dried glassware's were used in all the experiments.

Preparation of chromium doped Co₃O₄ nanoparticles

A homogeneous solution of Cr²⁺ and Co²⁺ was obtained by mixing appropriate amounts of CrCl₂·6H₂O and CoCl₂·6H₂O in double distilled deionized water. The solution of the diluted NH₃·H₂O (25%) was added to the above solution with continuous stirring till the pH 11 was reached. After stirring at room temperature for 30 min, the reaction mixture was reflux at 180°C for two hours. The product was aged for 24 h and the resulting precipitates were centrifuged, followed by washing with doubled distilled water. The sample was then dried at 80°C for 2 h and the obtained sample was further annealed at 400°C for 3 h. In this way, Cr:Co₃O₄ nanoparticles containing different concentrations of chromium (0, 1, and 5 mole%) were prepared and annealed at 400°C for 3 h.

Catalyst characterization

The crystal structure of the prepared materials was implemented by the X-ray diffraction (XRD, a Pananalytical's X'Pert Pro X-ray diffractometer, λ=1.5406 Å) in the range 2θ of 10-80° with scan rate of 10°/min and Cu Kα radiation, 40 KV. Surface morphology was achieved by applying Scanning electron microscopy (SEM) images were obtained on a JEOL: JSM-6490 LV Scanning Electron Microscope. Chemical composition was investigated by using energy dispersive X-ray (EDX) spectroscopy. The sample was heated for pre-treatment for 2 h under vacuum at 120°C before measurements. Then specific surface areas and pore size distributions were investigated from the consequence of N₂ adsorption-desorption measurement at 77 K (BELSORP MINI II) by using the BET (Brunauer-Emmett-Teller) and BJH (Barrett-Joyner Halenda). The spectrum of UV-Visible spectra was verified in absorption mode with a carry 100 spectrophotometer in the 200-800 nm regions.

Photocatalytic activity of chromium doped Co₃O₄ nanoparticles

The application of the synthesized product was predicted by photo degradation of methylene blue (MB) in presence of visible light radiation in a photocatalytic chamber. 200 mg quantity of prepared Co₂O₃ materials initially dissolved in 100 ml of 1 × 10⁻⁵ M, MB standard solution and mixture solution was stirred for 30 min in the dark condition in order for attaining the adsorption-desorption equilibrium. Finally, the solution was irradiated with visible light from the fluorescent lamp (9 W) in a photocatalytic chamber. The solution was agitated, during irradiation by using a magnetic stirrer and air was supply into the reaction mixture to implement a constant supply of oxygen. After the preferred time interaction, an aliquot amount of the solution was withdrawn, centrifuged and take its absorbance on a UV-visible spectrophotometer to measure the percentage degradation. The same procedure was reciprocated for 1% chromium doped cobalt oxide and 5% chromium doped cobalt oxide NPs also. The degradation efficiency of photocatalytic was measured by applied the following equation:

$$(\%) \text{ degradation} = \left\{ \left(\frac{A_0 - A_t}{A_0} \right) \times 100 \right\}$$

Where A₀ represents the initial absorbance of the dye solution and A_t; the absorbance after irradiation at a particular time t.

Results and Discussions

Nanostructure of chromium doped Co₃O₄ nanoparticles

The crystal structural and phase of the as prepared sample Co₃O₄ was recorded by XRD analysis as shown in Figure 1. All peaks have a good agreement with the standard spinel cubic Co₃O₄ suggesting that the sample produced is well crystallized Co₃O₄. However some small intense peaks correspond to CoO also found in the XRD patterns as an impurity. As presented curve in Figure 1a, XRD pattern, the intense peaks are consistent with the cubic spinel Co₃O₄ phase with space group Fd3m, (JCPDS No. 80-1535) perfectly, suggesting preferable formation of Co₃O₄. Peaks at 31.096°, 36.742°, 44.649°, 48.812°, 59.010, 64.920°, and 73.782° are assigned to the (220), (311), (400), (331), (511), (440) and (620) planes of the cubic spinel Co₃O₄, respectively. The crystallites size of Co₃O₄ was determined from the strongest peak (311) and calculated to be 21.9 nm according to the Scherer's equation [21]:

$$d = \frac{0.91\lambda}{\beta \cos \theta} \quad (1)$$

Where d is the average particle size of crystallites; λ is the X-ray wavelength; β is the full width at half maximum (FWHM) of the peak and θ the Bragg's angle thus confirming that the crystal size of Co₃O₄.

Structural, morphological and compositional analysis of as-prepared materials was accomplished by SEM and EDX investigated. Figure 2a exhibit the SEM image of Co₃O₄, formed by heating the precipitate, achieved by reaction of CoCl₂·6H₂O in the presence of ammonia in an aqueous medium. In the SEM image, spherical structures of Co₃O₄ nanoparticles have been observed. In the corresponding EDX spectrum Figure 2d the Co:O ratio in the product is contributed as 3:4, implying that the material is composed of Co and O elements in 3:4 ratio. The SEM image of 1% chromium doped cobalt oxide (1% Cr: Co₃O₄) NPs is displayed in Figure 2b. From the observation of the SEM image, the morphology of 1% Cr:Co₃O₄ NPs is similar to that of cobalt oxide; however there is no change in the shape and size. Corresponding EDX spectrum of 1% Cr: Co₃O₄ Figure 2e indicates that the nanoparticle is composed of chromium, cobalt and oxygen element. In the SEM image Figure 2c the morphology of the 5% chromium doped cobalt oxide (5% Cr:Co₃O₄) NPs is consist of spherical nanocrystals and micropores [22] but size is smaller to the

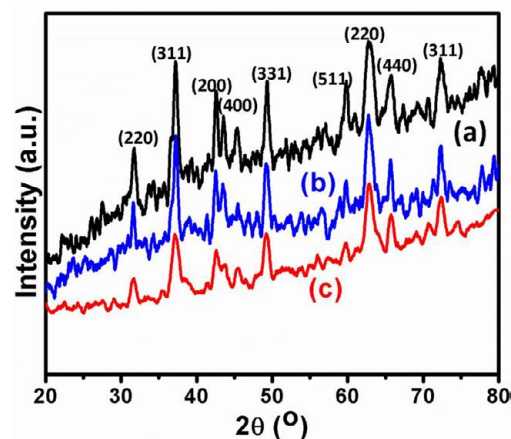


Figure 1: XRD graph of (a) Cobalt oxide (b) 1% Cr doped cobalt oxide (c) 5% Cr doped cobalt oxide.

other NPs. All together Figure 2f (the EDX spectrum) indicates that the particle is also composed of chromium, cobalt, and oxygen.

Nitrogen sorption measurements are carried out to further study of the surface and porosity of as-synthesized chromium doped Co₃O₄ materials. Typical nitrogen adsorption-desorption isotherms are demonstrated in Figure 3. These isotherms display type IV isotherms with H3 hysteresis loops, characteristics of mesoporous materials. The textural behaviour of prepared catalysts was also examined by the BET surface area, pore size distribution and total pore volume

measurements. The results are systematically shown in Table 1. It is observed from the Barrett-Joyner-Halenda (BJH) plot that the addition of dopants to the base Co₃O₄ photocatalyst leads to an increase in surface area. The observed order of considerable surface areas in terms of booster like chromium added is 5% Cr:Co₃O₄ > 1% Cr:Co₃O₄ > Co₃O₄, respectively. The large surface area of the doped materials might be associated to that metal ions contribution as additional nucleation sites during the precipitation and subsequent growth steps and this leads to solid materials with higher surface areas. The average pore diameter of the prepared samples is in the following sequence Co₃O₄ > 1% Cr:Co₃O₄ > 5% Cr:Co₃O₄. The addition of increase percentage of chromium over Co₃O₄ base catalyst caused a drastic decrease in average pore diameter Table 1. The lowest pore size is obtained over 5% Cr:Co₃O₄ doped cobaltite sample. Furthermore; it is remarkable to note that among doped catalysts, surface area increases and pore diameter decreases as percentage of chromium metal increases. Small pore diameters are obtained with sample having higher surface area.

In Figure 4, measurements of pore-size distributions by the BJH method are presented for all the materials. The graph indicates that the photocatalyst materials consumed broad pore size distributions in the mesoporous region, illustrating the volatile-sized mesopores in the photocatalyst structure. The 1% Chromium doped Co₃O₄ (1% Cr:Co₃O₄) materials shows a peak around 60 Å, but also a shoulder at a lower pore diameter of 90 Å. The 5% Chromium doped (5% Cr:Co₃O₄) materials reveals a peak around 120 Å. The un-doped Co₃O₄ nanoparticles reveal a peak at 90 Å as about the similar distribution profiles.

Optical and photocatalytic properties of chromium doped Co₃O₄ nanoparticles

The UV-Visible spectra of all the materials were recorded in the aqueous solution and direct band gap energy was calculated from the Tauc relation:

$$(\epsilon h\nu)^2 = P(E_g - h\nu) \quad (2)$$

Where ϵ is the molar extinction coefficient, h is plank constant, ν is the frequency of light, E_g is the band gap energy and P is the arbitrary constant. The plot of $(\epsilon h\nu)^2$ against energy of photon ' $h\nu$ ' shown sharp absorption edge of the powder catalyst and E_g was calculated by extrapolation of the linear region of the plot as shown in Figure 5. For

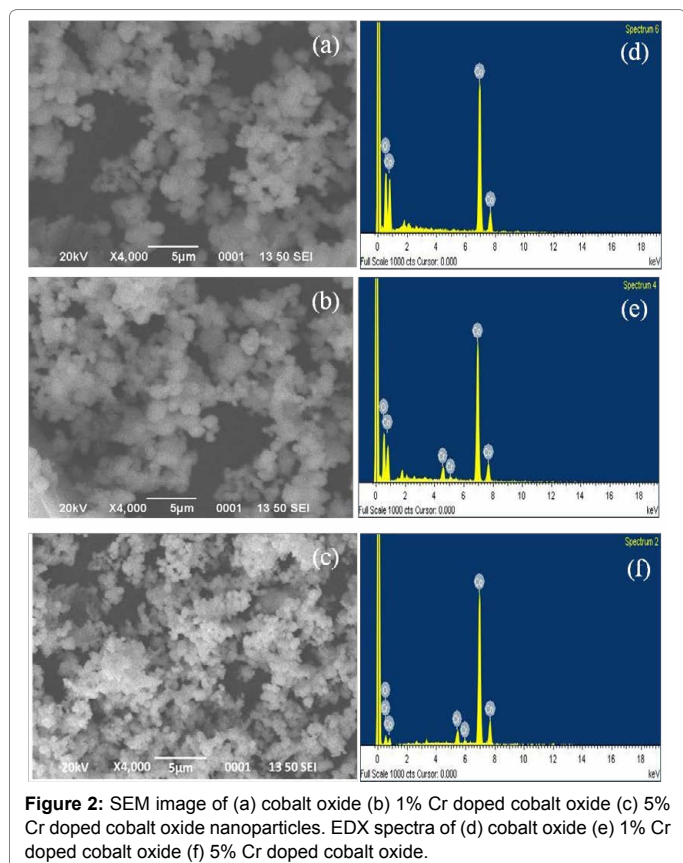


Figure 2: SEM image of (a) cobalt oxide (b) 1% Cr doped cobalt oxide (c) 5% Cr doped cobalt oxide nanoparticles. EDX spectra of (d) cobalt oxide (e) 1% Cr doped cobalt oxide (f) 5% Cr doped cobalt oxide.

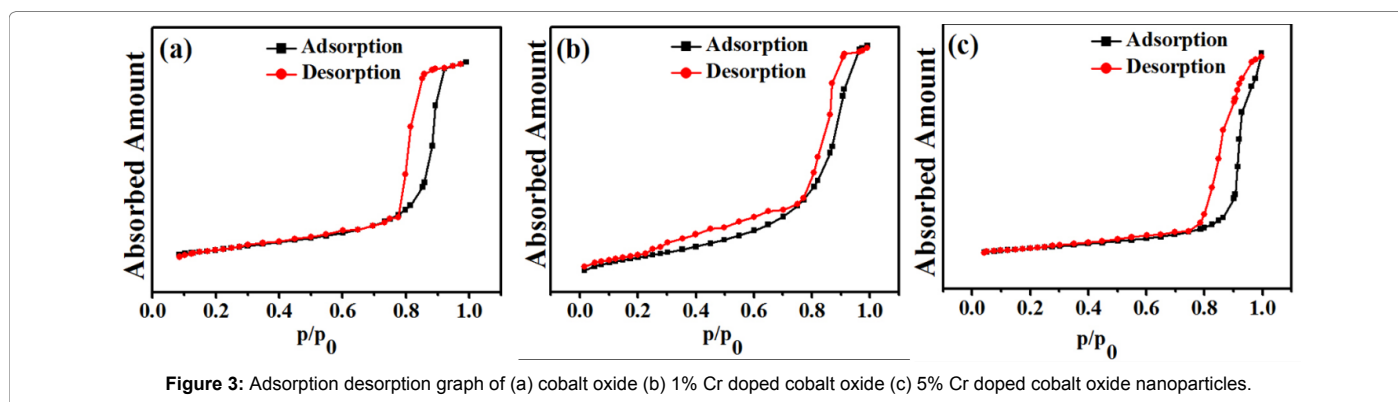


Figure 3: Adsorption-desorption graph of (a) cobalt oxide (b) 1% Cr doped cobalt oxide (c) 5% Cr doped cobalt oxide nanoparticles.

| Photocatalyst | Total surface area (m ² g ⁻¹) | Total pore volume (cm ³ g ⁻¹) | Average pore diameter (Å) | Crystallite size (nm) |
|--------------------------------|--|--|---------------------------|-----------------------|
| Co ₃ O ₄ | 54.79 | 0.293 | 122.4 | 21.9 |
| 1% chromium doped cobalt oxide | 79 | 0.2758 | 79.9 | 19.49 |
| 5% chromium doped cobalt oxide | 99.12 | 0.2726 | 60.6 | 14.23 |

Table 1: Textural property of the photocatalysts.

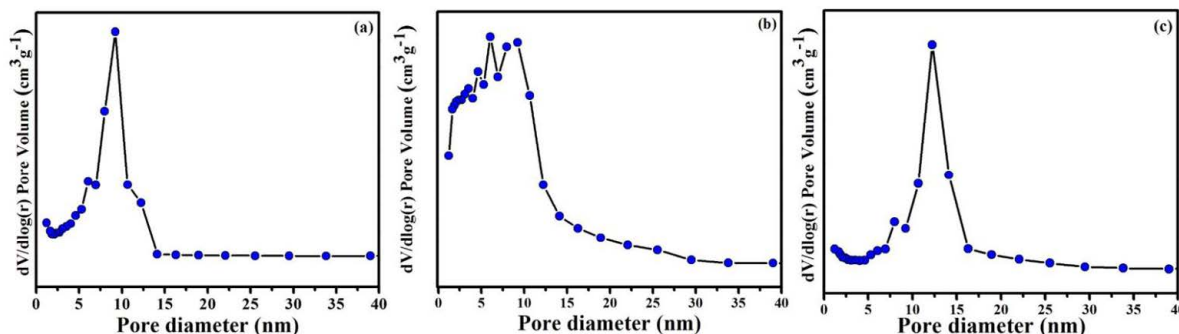


Figure 4: Pore size distribution of (a) cobalt oxide (b) 1% Cr doped cobalt oxide (c) 5% Cr doped cobalt oxide nanoparticles.

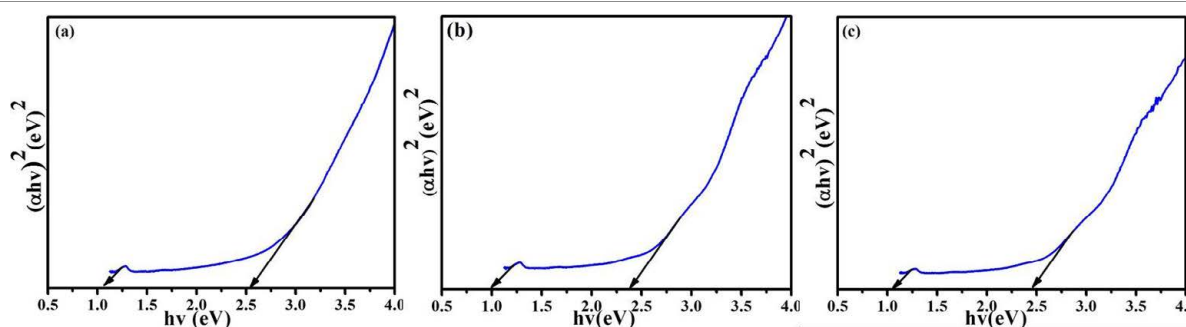


Figure 5: Band gap energy of (a) cobalt oxide (b) 1% Cr doped cobalt oxide (c) 5% Cr doped cobalt oxide nanoparticles.

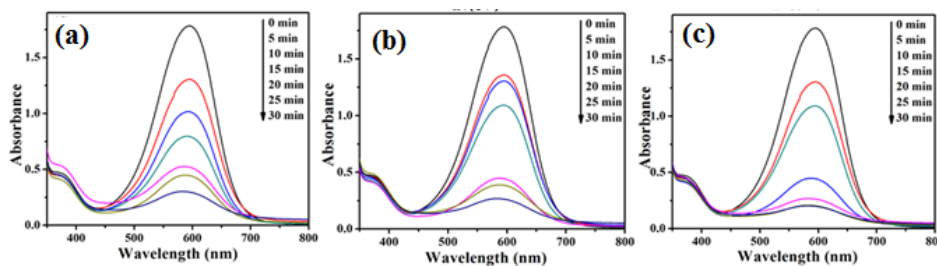


Figure 6: Absorption spectra of Methylene blue solution (100 ml 50 mg/L) in the presence of (a) 0.2 g Co₃O₄ (b) 0.2 g 1% Cr doped Co₃O₄ (c) 0.2 g 5% Cr doped Co₃O₄ catalyst.

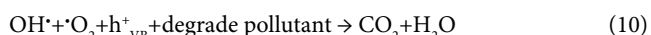
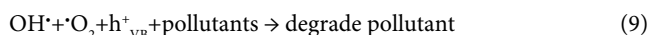
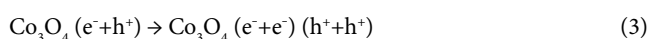
the chemically synthesized materials Co₃O₄, there were two types of optical transitions indicated at 1.05 (E_{g1}) and 2.53 eV (E_{g2}). However, change in the band gap energy of nanosized Co₃O₄ Cr doping and it may be due to Cr accommodation in the Fermi energy levels across the heterojunctions [23]. Generally the lower transitions of band gap are associate to O₂⁻→Co₃⁺ (E_{g1}) charge transfer and the higher band gap transitions are related with the O₂⁻→Co₂⁺ (E_{g2}) charge transfer processes [24]. The change in the E_{g2} (valence to conduction band excitation) of Co₃O₄ with 1.0, and 5.0% doped Cr was 2.44, and 2.37 eV respectively, and the experimental data its represented that 5.0% Cr:Co₃O₄ has the more advanced photocatalytic application in some oxidation process.

The photo degradation capability of organic pollutants by the above-synthesized Co₃O₄, 1% Cr:Co₃O₄ and 5% Cr:Co₃O₄ photo catalysts was calculated by measuring photo degradation performance of organic dye methyl blue (MB). In the current investigation, uninterrupted air bubbling was supplied to confirm the presence of O₂, which was used as an oxidizing agent. Figure 6a-6c represent the deviation in the UV-visible absorbance spectra of MB solution (50 mg/L) with different irradiation

time in the presence of prepared photo catalysts Co₃O₄, 1% Cr:Co₃O₄ and 5% Cr:Co₃O₄. Figure 6 illustrate the amount of degradation of the MB dye by Co₃O₄, 1% Cr:Co₃O₄ and 1% Cr:Co₃O₄ under the irradiation of visible light for 35 min time. It is noticeable from the UV-Visible spectra that photo degradation capacity of 5% Cr:Co₃O₄ is the highest and Co₃O₄ is the lowest while in the case of 1% Cr:Co₃O₄, it lies in between Co₃O₄ and 5% Cr:Co₃O₄ for the degradation of MB. Almost complete degradation of adsorbed dye molecules (~99%) was observed within 35 min using 5% Cr:Co₃O₄ nanoparticles. It is shown that the photocatalytic efficiency of semiconductor photo catalysts depends on various properties like band gap, phase/crystal structure, particle size, shape, surface area, surface defects and presence of bound molecules on the surface. The photocatalytic activity of Co₃O₄, 1% Cr:Co₃O₄ and 5% Cr:Co₃O₄ has a direct correlation with surface area [25]. The photocatalytic activity for 5% Cr:Co₃O₄ is the highest because its surface area is the highest (99.12 m²/g⁻¹), for Co₃O₄, it is the lowest because the surface area of the same is the lowest (54.79 m²/g⁻¹) while in the case of 1% Cr:Co₃O₄, it lies in between two samples, because the surface area of 1% Cr:Co₃O₄ (79.00 m²/g⁻¹) lies in between 5% Cr:Co₃O₄ and Co₃O₄.

The above data confirm that the photocatalytic activity of the materials has direct correlation with the surface area of the photocatalysts, along with the crystallinity of the materials. Apart from the high surface area, the presence of high density of oxygen vacancies and/or defects in the 5% Cr:Co₃O₄, calcinated at 400°C, played an important role on high photo-oxidation capacity. The band gap energy of Co₃O₄ is too high to be excited by visible light. However, its band gap can be manipulated to such an extent where visible light induced photocatalysis could take place effectively. Such modification can be achieved by doping or by the addition of other transition metal to Co₃O₄ to make diluted like 1% Cr:Co₃O₄ and 5% Cr:Co₃O₄. Figure 5 shows that the band gap of pure Co₃O₄ (2.7eV value) is lowered to 2.5 eV for the 1% Cr:Co₃O₄ and further to 2.4 eV in the case of 5% Cr:Co₃O₄. The improvement of photocatalytic activity of 1% Cr:Co₃O₄ and 5% Cr:Co₃O₄ NPs could be achieved due to a decrease of band gap values, which in turn cause an increase of electron-hole formation under visible light irradiation.

The fact that the synthesized photocatalysts adsorb significantly more dye during the reaction, suggests a possible adsorption-desorption mechanism. Visible light irradiation generates an electron-hole pair on the surface of above-prepared Co₃O₄, 1% Cr:Co₃O₄, and 5% Cr:Co₃O₄ catalysts. The electron-hole pair enables the formation of some intermediate radicals such as hydroxyl radicals, hydroperoxyl radicals and superoxide radical anions in the catalytic solution by their interaction with water and oxygen from the supplied air. Continuous air bubbling facilitates the formation of these radicals; mainly the hydroxyl radicals, which participates directly in the oxidative photodegradation of dye molecules. As the degradation involves adsorption followed reaction, the adsorbed dye molecules can easily interact with the photo-generated oxidizing radical species, resulting in the degradation of dye. The high photocatalytic activity of 1% Cr:Co₃O₄ and 5% Cr:Co₃O₄ may be due to the diminishing of the recombination of electron-hole pairs in these materials and hence encouraging their catalytic activity. In fact, a large amount of oxygen vacancies present in 1% Cr:Co₃O₄ and 5% Cr:Co₃O₄ function as electron acceptors and trap electrons of the conduction band, thus decreasing the rate of recombination of electrons and holes and increasing rate of photo catalysis [26].



Since the band gap of Co₃O₄ becomes narrower and narrower while oxygen vacancies go richer and richer by the addition of 1% and 5% chromium transition metal, the photocatalytic activity of 1% Cr:Co₃O₄ found better than Co₃O₄ while in the case of 5% Cr:Co₃O₄, it is the best among three.

The photocatalytic degradation of Methylene blue under visible light irradiation using Co₃O₄, 1% Cr:Co₃O₄ and 5% Cr:Co₃O₄ materials is an example of diluted semiconductor catalysis and these reactions seldom follow the proper rate law model and hence it is inherently difficult to formulate a rate equation from the observed data. The

kinetic study of the synthesized catalyst for the photo-degradation of MB was measured by Langmuir-Hinshelwood eqn. (11)

$$\ln \frac{C}{C_0} = -kt \quad (11)$$

Here C₀ is the initial concentration of dye solution, C the concentration after time t and k is the rate constant [27]. In order to further investigate the effect of the chromium doping level on the catalytic activities of the nanoparticle catalysts, Figure 7 shows the curves of C/C₀ at various time points after being treated with different catalysts. A near linear correlation between C/C₀ and time was observed. A graph has been plotted between ln C/C₀ versus t (Figure 8) where rate constant k can be determined by the slope of the fitting curve. From the above graph, the rate constant values for Co₃O₄, 1% Cr:Co₃O₄ and 5% Cr:Co₃O₄ catalysts have been determined as 0.057, 0.072 and 0.083 min⁻¹ respectively. The results indicate that 5% Cr:Co₃O₄ is an excellent photo catalyst and photocatalytic activity of these materials follows the following trend; 5% Cr:Co₃O₄ > 1% Cr:Co₃O₄ > Co₃O₄ for degradation of dye MB (Figure 8).

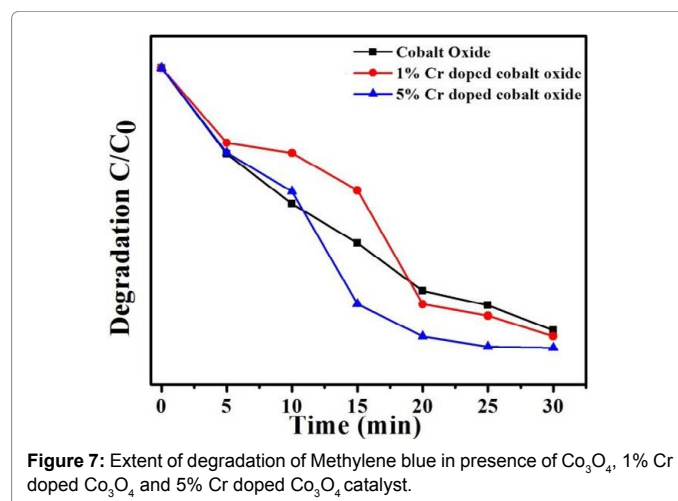


Figure 7: Extent of degradation of Methylene blue in presence of Co₃O₄, 1% Cr doped Co₃O₄ and 5% Cr doped Co₃O₄ catalyst.

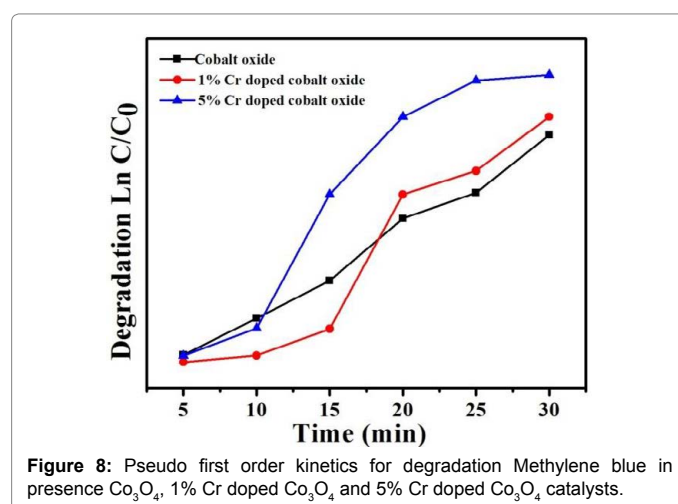


Figure 8: Pseudo first order kinetics for degradation Methylene blue in presence Co₃O₄, 1% Cr doped Co₃O₄ and 5% Cr doped Co₃O₄ catalysts.

Conclusion

In summary, Co₃O₄, 1% Cr:Co₃O₄, and 5% Cr:Co₃O₄ nanoparticles have been successively synthesized by homogeneous precipitation method. XRD and SEM studies revealed a cubic, spherical like the structure of Co₃O₄, 1% Cr:Co₃O₄, and 5% Cr:Co₃O₄ nanoparticles

with respectively crystallites size of 21, 19 and 14 nm at calcination temperatures of 400°C. The photocatalytic activity results revealed that the Co₃O₄, 1% Cr:Co₃O₄, and 5% Cr:Co₃O₄ nanoparticles formed by calcination at 400°C are effective photocatalysts, however, 5% Cr:Co₃O₄ has the highest and Co₃O₄ the lowest photocatalytic activity for degradation of methylene blue. The UV-visible absorption shows that the band gap of Co₃O₄ (2.7 eV) is decreased to 2.5 eV for 1% Cr:Co₃O₄ and further to 2.4 eV for 5% Cr:Co₃O₄ nanoparticles, therefore the photocatalytic activity of 1% Cr:Co₃O₄ is higher than Co₃O₄ while the same for 5% Cr:Co₃O₄ is the highest among three samples for degradation of MB under visible light irradiation.

References

1. Robinson I, Ung D, Tan B, Long J, Cooper AI, et al. (2008) Size and shape control for water-soluble magnetic cobalt nanoparticles using polymer ligands. *Journal of Materials Chemistry* 18: 2453-2458.
2. Trudel S, Jones CH, Hill RH (2007) Magnetic properties of nanocrystalline iron oxide/amorphous manganese oxide nanocomposite thin films prepared via photochemical metal-organic deposition. *Journal of Materials Chemistry* 17: 2206-2218.
3. Noor S, Hakim M, Sikder S, Hoque SM, Maria KH, et al. (2012) Magnetic behavior of Cd²⁺ substituted cobalt ferrites. *Journal of Physics and Chemistry of Solids* 73: 227-231.
4. Guo D, Fan X, Chai G, Jiang C, Li X, et al. (2010) Structural and magnetic properties of NiZn ferrite films with high saturation magnetization deposited by magnetron sputtering. *Applied Surface Science* 256: 2319-2322.
5. Lu AH, Salabas EL, Schüth F (2007) Magnetic nanoparticles: synthesis, protection, functionalization, and application. *Angewandte Chemie International Edition* 46: 1222-1244.
6. Menini L, Pereira MC, Parreira LA, Fabris JD, Gusevskaia EV (2008) Cobalt- and manganese-substituted ferrites as efficient single-site heterogeneous catalysts for aerobic oxidation of monoterpene alkenes under solvent-free conditions. *Journal of Catalysis* 254: 355-364.
7. Rajabi F, Karimi N, Saidi MR, Primo A, Varma RS, et al. (2012) Unprecedented selective oxidation of styrene derivatives using a supported iron oxide nanocatalyst in aqueous medium. *Advanced Synthesis & Catalysis* 354: 1707-1711.
8. Gawas U, Verenkar VMS, Patil DR (2011) Nanostructured ferrite based electronic nose sensitive to ammonia at room temperature. *Sensors & Transducers*. Toronto 134: 45-55.
9. Gupta AK, Gupta M (2005) Synthesis and surface engineering of iron oxide nanoparticles for biomedical applications. *Biomaterials* 26: 3995-4021.
10. Wickham D, Goodenough J (1959) Suggestion concerning magnetic interactions in spinels. *Physical Review* 115: 1156.
11. Sawatzky G, Van Der Woude F, Morrish A (1969) Recoilless-fraction ratios for Fe 57 in octahedral and tetrahedral sites of a spinel and a garnet. *Physical Review* 183: 383.
12. Lu Y, Wang Y, Zou Y, Jiao Z, Zhao B, et al. (2010) Macroporous Co₃O₄ platelets with excellent rate capability as anodes for lithium ion batteries. *Electrochemistry Communications* 12: 101-105.
13. He T, Chen D, Jiao X, Wang Y, Duan Y (2005) Solubility-controlled synthesis of high-quality Co₃O₄ nanocrystals. *Chemistry of materials* 17: 4023-4030.
14. Gu F, Li C, Hu Y, Zhang L (2007) Synthesis and optical characterization of Co₃O₄ nanocrystals. *Journal of crystal growth* 304: 369-373.
15. Dutta P, Seehra M, Thota S, Kumar J (2007) A comparative study of the magnetic properties of bulk and nanocrystalline Co₃O₄. *Journal of Physics: Condensed Matter* 20: 015218.
16. Cao AM, Hu JS, Liang HP, Song WG, Wan LJ, et al. (2006) Hierarchically structured cobalt oxide (Co₃O₄): the morphology control and its potential in sensors. *The Journal of Physical Chemistry B* 110: 15858-15863.
17. Park J, Shen X, Wang G (2009) Solvothermal synthesis and gas-sensing performance of Co₃O₄ hollow nanospheres. *Sensors and Actuators B: Chemical* 136: 494-498.
18. Chen Y, Zhang Y, Fu S (2007) Synthesis and characterization of Co₃O₄ hollow spheres. *Materials Letters* 61: 701-705.
19. Morsali A, Monfared HH, Morsali A (2009) Synthesis and characterization of Mn₃O₄ nanoparticles via thermal decomposition of a new synthesized hydrogen bonded polymer. *Journal of Molecular Structure* 938: 10-14.
20. Wang G, Shen X, Horvat J, Wang B, Liu H, et al. (2009) Hydrothermal synthesis and optical, magnetic, and supercapacitance properties of nanoporous cobalt oxide nanorods. *The Journal of Physical Chemistry C* 113: 4357-4361.
21. Pandey G, Dixit S (2011) Growth mechanism and optical properties determination of CdS nanostructures. *The Journal of Physical Chemistry C* 115: 17633-17642.
22. Nehru L, Swaminathan V, Sanjeeviraja C (2012) Rapid synthesis of nanocrystalline ZnO by a microwave-assisted combustion method. *Powder technology* 226: 29-33.
23. Zhang H, Pokhrel S, Ji Z, Meng H, Wang X, et al. (2014) PdO doping tunes band-gap energy levels as well as oxidative stress responses to a Co₃O₄ p-type semiconductor in cells and the lung. *Journal of the American Chemical Society* 136: 6406-6420.
24. Meher SK, Rao GR (2011) Effect of microwave on the nanowire morphology, optical, magnetic, and pseudo capacitance behavior of Co₃O₄. *The Journal of Physical Chemistry C* 115: 25543-25556.
25. Barick K, Sharma P, Mukhija A, Sainis J, Gupta A, et al. (2015) Effect of cetylpyridinium chloride on surface passivation and photocatalytic activity of ZnO nanostructures. *Journal of Environmental Chemical Engineering* 3: 1346-1355.
26. Saravanan R, Karthikeyan S, Gupta V, Sekaran G, Narayanan V, et al. (2013) Enhanced photocatalytic activity of ZnO/CuO nanocomposite for the degradation of textile dye on visible light illumination. *Materials Science and Engineering: C* 33: 91-98.
27. Kumar KV, Porkodi K, Rocha F (2008) Langmuir-Hinshelwood kinetics—a theoretical study. *Catalysis Communications* 9: 82-84.